# PORE SPACE CHARACTERIZATION OF COATING LAYERS

Martti Toivakka
Kjell Nyfors
Laboratory of Paper Chemistry
Åbo Akademi University
FIN-20500 Turku
FINLAND
Tel. +358-2-2154625
Fax +358-2-2153226
Email: Martti.Toivakka@abo.fi
Kjell.Nyfors@abo.fi

## ABSTRACT

Although coating and pore structures are commonly discussed in context of paper coating performance, the actual microscopic geometry of the void space still remains largely unknown. This paper presents a technique to partition a void space of porous material into unambiguously defined collection of individual pores. The characterization technique is based on three-dimensional image analysis and it can be applied to both experimental and model packing data. The technique produces useful new information of microscopic properties of pore spaces including distributions of pore size, surface area, pore connectivity, pore surface-to-volume ratio, throat-to-surface area ratio as well as fractal structural parameters. Additionally, the technique creates a topological model of the pore space that can be used as a starting point for predictions of transport processes in porous structures, e.g. short time absorption of printing inks.

Basic ideas and accuracy of the characterization technique are demonstrated by analyzing ordered lattice packings of cubic and hexagonal arrangements. Pore spaces in random packings of mono- and polydisperse spherical particles are characterized. The results quantify differences in pore structures caused by changes in particle size distributions. An understanding of microscopic pore structures in coating layers enables papermaker to improve and optimize coating formulations by using, e.g. pigment-blending.

## INTRODUCTION

Most physical and functional properties of pigment coated papers are influenced, to a greater or lesser degree, by the porous structure of coating layer. For example, number and size of micro voids contribute to macroscopic properties such as brightness, light scattering efficiency and opacity. The void structure also affects the flow of liquids and gases in a coating. Absorption of inks and fountain solutions during printing is controlled by the structure of the pore space near coating surface.

The porous structure of coating layer depends on coating color formulation, used pigments and their combinations, chemical additives (e.g. associative thickeners), and coating color application and drying processes. There is some agreement on the type of coating structure that is desirable for satisfactory coated paper performance, but a detailed knowledge of existing and optimal structures is lacking at present time [1]. In the context of coating pigments, particle size distributions are commonly quoted since they are measurable. However, for the end use performance a more important aspect is the pore space that is created by the packed pigment particles. In practice, it is difficult to predict the kind of pore space that is created by a certain particle size distribution. Macroscopic properties of a pore space such as porosity, specific surface area and permeability can easily be measured experimentally, but do not provide the necessary level of detail [2]. Local variations in a pore structure generate physical effects, e.g. mottle, that cannot be explained with simple macroscopic measurements. It is, therefore, of fundamental interest to study and understand what type of microscopic pore structures are advantageous for the papermaker.

If one wants to understand mechanisms of dynamic transport phenomena in paper coatings, a detailed description of the porous structure is required. Absorption of printing inks and fountain solutions cannot be predicted by using models based on single parameters such as porosity and permeability. Therefore, the detailed description must include microscopic information, e.g. pore size distribution, pore geometry and connectivity.

A common experimental method to obtain pore size distributions of porous media is Mercury intrusion porosimetry. One limitation of this method is that it does not take into account the real topology of a pore structure, but is based on a simplified model consisting of parallel capillaries [2]. The information obtained does not allow one to gain a fundamental understanding of microscopic mechanisms that control, e.g. ink-setting. Despite the shortcomings, Mercury intrusion porosimetry remains a useful experimental method to characterize porous structures if used with discretion.

Pore-Cor is a simulation tool that fits a [10x10x10] pore array model to experimental data obtained by Mercury porosimetry [3, 4]. The pores in the model are connected to each other with cylindrical throats and have a maximum connectivity of 6. Although the model is an improvement over the parallel capillary model and useful information can be extracted with it, the model still represents a somewhat simplified view of porous media.

Kwiecien *et al.* and Zhao *et al.* have used multi-orientation scanning through three-dimensional digitized samples of real porous media to characterize pore spaces [5, 6]. Their approach sought to partition a pore space into a collection of pores and necks. The identification of necks was carried out by finding minima in projected pore radii. For reliable neck identification the search has to be performed in sufficient number of orientations, which makes the characterization difficult. Zhao's application required scannings in a minimum of nine orientations [6].

With recent improvements in magnetic resonance imaging it is now possible to obtain three-dimensional images of pore spaces [7]. These images can readily be processed with various image analysis algorithms. Especially morphological erosion, first suggested by Lin and Cohen [8], has been found to be a useful method to analyze three-dimensional data. The first implementation was proposed by Thovert *et al.*, who used both morphological thinning and skeletonization to determine deformation retract of porous media [9]. This provided information on the connectedness of a void space, while shape, size and surface area information was not

obtained. Baldwin *et al.* introduced a more rigorous algorithm to characterize volume images [7]. Their approach partitioned a pore space into a collection of individual pores separated by volumeless necks. The necks were defined as in Dullien [1] to be the minima in the hydraulic radius (the ratio of cross-sectional area to wetted perimeter) between two pores. This definition is substantial, as hydraulic radius is inversely proportional to the pressure required for an interface between two immiscible fluids to pass through a constriction according to Laplace's equation of capillarity [10].

Properties of ordered and random sphere packings have been subject of research for many decades [11–14]. Although much is known about these packings, the detailed geometry of the pore space is only known for ordered systems. Eksi and Bousfield generated random packings of spherical particles with a computer model and characterized the corresponding pore spaces [15]. A limitation of their work was the tetrahedral pore definition, which imposes a connectivity of 4 to all the identified pores.

The present work builds on ideas of [7–9, 15] by identifying and correcting some of the shortcomings in earlier approaches. The objective is to demonstrate the usefulness of a pore space characterization technique that is based on three-dimensional image analysis. In the absence of experimental input data, the technique is applied to computer generated packings of spherical particles. A related paper [16] focuses on prediction of liquid flow in the topological model of the pore space obtained with the technique described in this paper.

## CHARACTERIZATION TECHNIQUE

The characterization technique partitions a void space into a collection of unambiguously defined pores. The pore definition is the one proposed by Dullien [10]: a pore is bounded by pore-solid interfaces and volumeless throats. The latter are defined as local minima in the hydraulic radius when moving from one pore to an adjacent one. The basic characterization procedure based on the approaches of [7–9] is outlined below. The shortcomings of previous algorithms are highlighted and important improvements are proposed. The technique presented here differs from the previously published ones by eliminating directional erosion, by filtering false local maxima in the eroded image and by improving calculation of pore statistics. These changes are significant; without them the number of false pore identifications can be considerable and pore surface area estimations unreliable.

The pore space characterization involves the following steps.

1. **Data input.** The starting point for an analysis is a three-dimensional computer representation of a sample. This can be obtained either experimentally through use of e.g. magnetic resonance imaging, or through sampling of a mathematical model packing. Unfortunately, at present time the resolution of computer tomography is extending only to about 1μm, which is not enough to characterize pigment coating layers. However, the analysis of void spaces in base sheets should be possible with existing techniques. Due to the lack of experimental input data, current work analyzes computer generated mathematical model packings.

2. **Binary volume image generation.** The pore identification procedure starts by dividing the input data into small three-dimensional cubic unit volumes, voxels ("three-dimensional pixels"). Then, voxels located in the solid matrix (pigment and latex) are identified and

labeled to separate them from voxels belonging to the void space. If input data is a gray scale volume image, e.g. experimental computer tomography data, thresholding of gray values can be used to generate the initial binary volume image. For a mathematical model packing of spheres all voxels, whose center-points fall inside any of the spheres in the packing, are identified as belonging to the solid phase. The initial packed particle structure and a subsection of the corresponding binary image are illustrated in **Figures 1a-c**. Two-dimensional images are used for clarity.

3. **Erosion of void space.** The characterization continues by applying morphological erosion, a common image analysis operation, to the pore space of the binary volume image. The erosion is initialized by first eroding all voxels that are connected to the solid phase. In the second iteration all voxels connected to the ones eroded initially are eroded. Two voxels are considered as being connected to each other if they share at least one common corner. The erosion process is continued layer by layer until all voxels in the pore space have been eroded. During the erosion voxels are assigned erosion values that correspond to the iteration that eroded them. **Figure 1d** illustrates the erosion process. Each successive erosion layer is drawn in a darkening shade of gray.

   *Elimination of directional erosion.* Erosion algorithms used in earlier works have shortcomings that are worth investigating. A voxel is surrounded by 26 connected neighbors that can be classified into three groups. The six nearest neighbors share a common face with the center voxel corresponding to a voxel center-to-center distance of 1 (made dimensionless with the voxel size). The twelve secondary nearest neighbors share a common edge with the center voxel, which corresponds to a voxel center-to-center distance of $\sqrt{2}$. The remaining eight connected neighbors share a common corner with the center voxel and are located at a voxel center-to-center distance of $\sqrt{3}$. Standard erosion algorithms proceed by eroding either the 6, 18 or all 26 nearest neighbors during each erosion operation. All the three algorithms lead to a non-uniform erosion; the erosion proceeds at different speeds in different angular directions in the image. This can have undesired consequences since erosion values of an eroded pore space do not relate to the true geometry of that pore space. Additionally, interfaces separating pores will be built preferentially in erosion angles rather than following the plane that defines the minimum hydraulic radius. The present work eliminates the directional erosion by using vectors instead of integers as erosion values. Initially, all voxels belonging to the solid phase are assigned null vectors. In the subsequent erosion of pore space, each voxel that is eroded is assigned a vector that points to the nearest solid phase voxel. The erosion still needs to be done in an iterative fashion in order to ensure that the shortest distance to the solid phase is found for each eroded voxel. If computer-generated packing of spheres is used as input data into the analysis, an alternative erosion algorithm can be used. In this case, shortest distances to solid surfaces can be calculated exactly since sphere center coordinates and radii are known.

4. **Identification of pore centers.** After the erosion operation a voxel's erosion value reflects the shortest distance from that voxel to the solid matrix. Therefore, points that are maximally distant from the solid phase can be identified as local maxima in the eroded image. These points are chosen as pore centers for the subsequent void space partitioning. The pore centers are indicated by black arrows in **Figure 1e**.

   *Elimination of false pore centers*. Due to digitalization of input data it is possible that a number of "false local maxima" are created in the eroded image. Two examples are shown in Figure 1e for a two-dimensional image. The false maxima are indicated with patterned arrows. If false maxima are not eliminated a number of false pores in narrow passages of the void space are created. Current work eliminates the problem by applying a filter to the local neighborhood of a potential pore center. The filtering algorithm makes decisions to keep or discard a pore center based on the erosion values of the voxels found in the local neighborhood. A local maximum does not correspond to a true pore center if a voxel with

higher erosion value than that of the local maximum is found in the immediate neighborhood. It is worth to note that the problem of non-uniform erosion discussed earlier also complicates the filtering procedure. False maxima are generated that are difficult to differentiate from those that should not be eliminated.

5. **Partitioning of pore space.** After identification of pore centers the pores themselves can be built up by assigning neighboring erosion layers to each pore center in an iterative fashion. During partitioning the expanding pores are separated from each other at the points of minimum hydraulic radius. The separation is an automatic result of the initial erosion process; voxels in narrow passages of the void space were eroded earlier than their local neighborhood and, therefore, will be the last ones to be assigned to pores. After all void space voxels have been processed, the void space has been unambiguously divided into individual pores. Each pore consists of a collection of connected voxels and is bounded by solid phase voxels and voxels belonging to neighboring pores. **Figure 1f** shows the partitioned pore space. The solid phase is white and the identified pores are shown in different shades of gray.

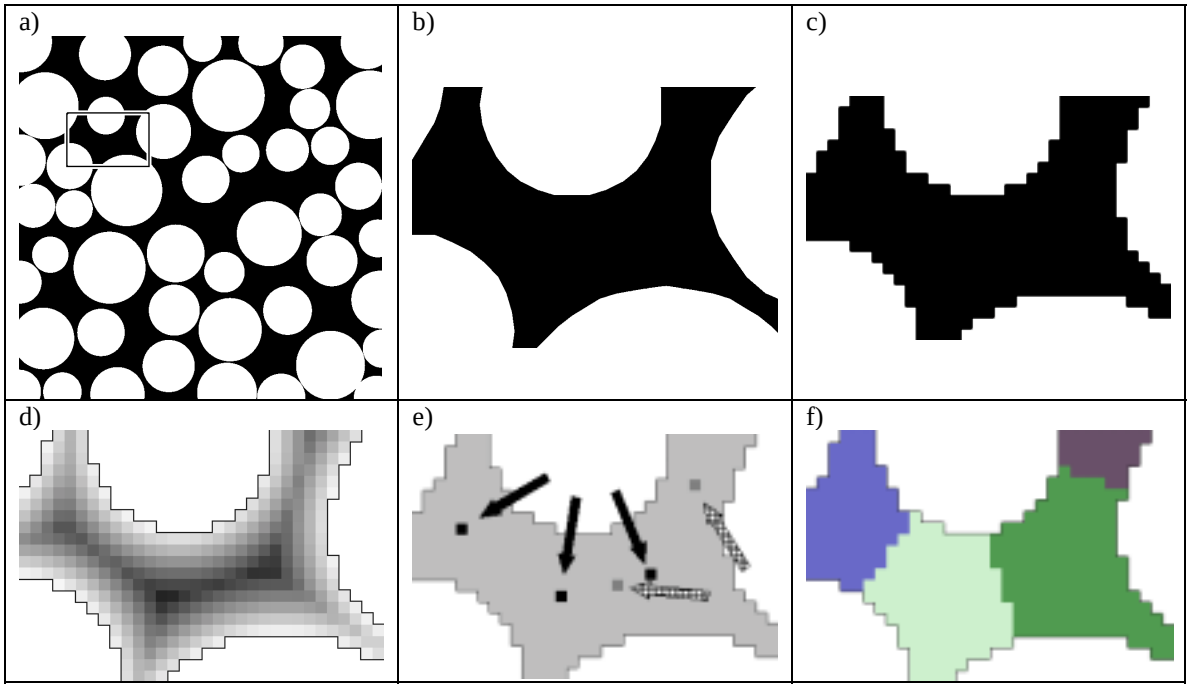


***Figure 1. Pore identification of a two-dimensional packing. (a) Packed structure that is used as input packing data. White is the solid phase (pigments). (b) Enlargement of a subarea in (a). (c) Digitized input data. (d) Erosion of pore space. Each successive erosion layer is drawn in a darkening shade of gray. (e) Pore center pixels that are maximally distant from the solid phase. Black and patterned arrows indicate correct and false pore centers, respectively. (f) Partitioned pore space after pore center expansion.***

6. **Calculation of pore space statistics.** Knowing the number and positions of voxels defining each pore in the partitioned void space, it is possible to calculate several measures that characterize pores. The measures include pore volume, equivalent spherical radius, equivalent hydraulic radius, internal surface area, throat area (area in contact with other pores), coordination number (connectivity to neighboring pores) and measures of pore form and orientation. Since these quantities are known for all the pores the results can also be expressed as statistical distributions. Additionally, macroscopic, "bulk" properties such as porosity and total surface area can be calculated. The partitioned pore space can also be used as a starting point for simulation of fluid flow in the porous structure. For one approach in this direction see the companion paper [16].

   *Improving the accuracy of statistics.* Although the calculation of pore statistics is relatively trivial, care has to be taken when calculating pore surface areas from voxel data. A simple way to calculate surface area adds up all voxel faces that are in contact with the solid phase. This can, however, greatly overestimate the true surface area. On the other hand, if each interface voxel is given an area contribution of 1, the total area can be significantly underestimated. In the current work a more accurate procedure to estimate surface area was developed. By taking into account the exposed faces of the neighboring voxels of a surface voxel, an improved estimate of the true surface area contribution can be obtained.

## RESULTS AND DISCUSSION

### Results of ordered packings

*Cubic packing*

In the first part of the results we demonstrate the accuracy of the characterization technique by applying it to well known ordered lattice packings, namely cubic and hexagonal packings of monodisperse spherical particles.

**Figure 2a** shows cubic packing of 27 spheres of radius 1.1 with nearest neighbor interparticle center-to-center separation of 2.0 (particle overlap of 0.2). The pore space corresponding to the packing as characterized by the proposed technique is shown in **Figure 2b**. The pores are represented by collections of small three-dimensional cubic unit volumes, voxels. Voxels of same color belong to the same pore. **Figure 2c** shows one pore in detail. In this figure the voxels that belong to throats, i.e. are in contact with other pores, are highlighted in different colors. In **Figure 2d** the connectivity of the pore space is illustrated by drawing the pore centers as large spheres, pore throats as pairs of small green spheres and connections as red strings of small spheres. As can be seen in Figure 2b the pore space is correctly partitioned into separate pores at the points of minimum hydraulic radius when moving from one pore to another.

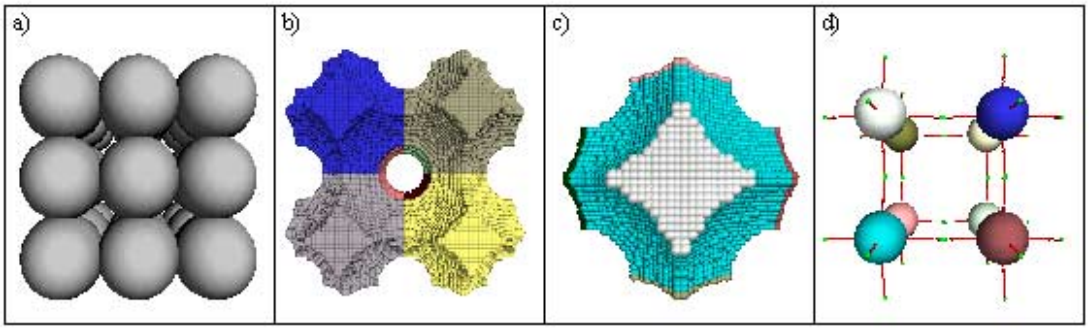


***Figure 2. Cubic packing (a), its pore space (b), an individual pore with throats (c) and the connection graph (d). Particle radius is 1.1 and interparticle center-center separation 2.0 (particle overlap 0.2).***

In order to verify correctness and accuracy the characterization technique three cubic packings were analyzed and results compared with the analytic expressions of pore parameters. The comparison data is summarized in **Table 1**. All the calculated statistics agree within 5% accuracy. Of course, the accuracy is dependent on the sampling resolution (how many voxels are used per unit length) and it can be improved with the expense of using more computing resources.

| | Particle radius in packing | | | | | |
|---|---|---|---|---|---|---|
| | 1.0 | | 1.1 | | 1.2 | |
| Pore statistic: | Model | Analytic | Model | Analytic | Model | Analytic |
| Volume | 3.81 | 3.81 | 2.62 | 2.62 | 1.62 | 1.62 |
| Coordination number | 6 | 6 | 6 | 6 | 6 | 6 |
| Surface Area | 13.07 | 12.57 | 11.28 | 11.06 | 8.99 | 9.05 |
| Throat area | 5.04 | 5.15 | 2.64 | 2.67 | 1.26 | 1.18 |

***Table 1. Comparison of analytic and characterization data for the pore space of cubic packing. Interparticle nearest neighbor center-to-center separation is 2.0. Sampling resolution is 20 voxels/unit length.***

*Hexagonal close packing (HCP)*

The other ordered packing that was analyzed was hexagonal close packing shown in **Figure 3a**. HCP is the closest ordered packed structure in three dimensions and also one that is common in nature [11]. In HCP one particle has 12 closest neighbors: 6 in the same plane and 3 above and below. There are two types of voids, smaller concave-tetrahedrons and larger concave-cubes. The number of smaller voids is twice that of the larger, which in turn is equal to the number of particles in the packing. The pore space in the HCP as partitioned by the proposed algorithm is shown in **Figure 3b**. The two types of pores are correctly identified and shown in **Figure 3c**. The large and small voids have the correct coordination numbers (connectivities) 8 and 4, respectively. The skeleton illustrating the void connections is shown in **Figure 4**. In this figure the void sizes are drawn with large spheres whose volumes are proportional to those of the corresponding voids. The figure reveals the clearly more complex pore structure of HCP when compared to the simple cubic packing.

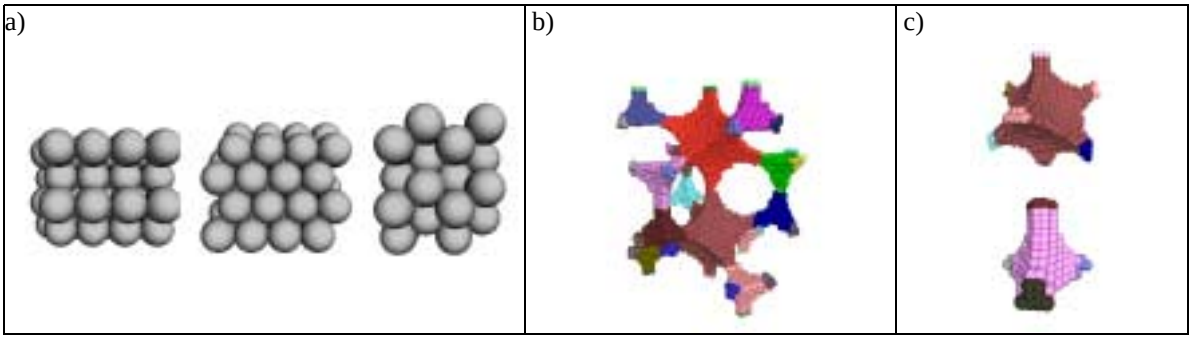


***Figure 3. Hexagonal close packing (a), its pore space (b) and the two different types of pores (c). Particle radius is 1.1 and closest neighbor center-to-center separation 2.0 (particle overlap 0.2).***

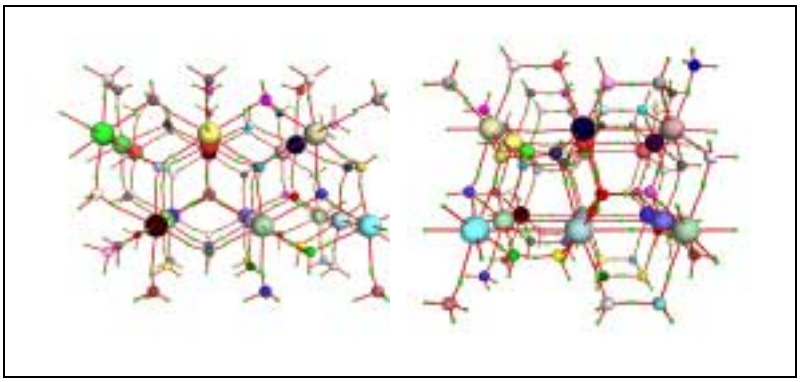

***Figure 4. Two views of the pore connections in the hexagonal packing shown in Figure 3a.***

**Table 2** compares the calculated and analytical values of pore statistics for HCP. Again, the agreement is good. The accuracy is somewhat reduced when compared to the cubic packing, especially in the throat area calculation. This is caused by the fact that most connections between pores in HCP are not parallel with the primary x-, y- or z-axis. Therefore, the use of cubic unit volumes that are aligned with the axis tends to increase the error in area calculations. This is not a problem since, as noted above, the resolution of the sampling can be increased until consistent results are obtained. An alternative approach to improve accuracy would be to rotate the input packing data, then repeat the calculations and average the results.

| | Particle radius in packing | | | | | | | |
|---|---|---|---|---|---|---|---|---|
| | 1.0 | | | | 1.1 | | | |
| | Model | | Analytic | | Model | | Analytic | |
| Pore statistics: | Large | Small | Large | Small | Large | Small | Large | Small |
| Volume | 1.04 | 0.20 | 1.05 | 0.21 | 0.40 | 0.042 | 0.40 | 0.043 |
| Coordination number | 8 | 4 | 8 | 4 | 8 | 4 | 8 | 4 |
| Surface Area | 8.53 | 2.30 | 8.16 | 2.20 | 5.19 | 1.05 | 4.83 | 1.04 |
| Throat area | 1.43 | 0.66 | 1.29 | 0.65 | 0.12 | 0.061 | 0.13 | 0.066 |

***Table 2. Comparison of analytic and characterization data for hexagonal packing. Closest neighbor center-to-center separation is 2.0. Sampling resolution is 20 voxels/unit length.***

## Results of random packings

*Pore space in monodisperse model packing*

Eksi and Bousfield have previously developed a computer model that simulates dewatering of coating layers and generates three-dimensional packed structures of spherical particles [15]. They also report the following statistics for packings: total porosity, porosity and surface roughness as a function of coating thickness, average pore radius and frequency distribution of pore radius.

The pore space characterization technique of present work was applied to the model packing used in the published work of Eksi and Bousfield. The packing structure of monodisperse spheres with 0.5μm diameter that was used as input data is shown in **Figure 5a**. The complex pore structure of the packing is apparent in **Figure 5b**, which shows a 0.5μm thick slice through the middle of the analyzed pore space. The complexity is further illustrated in **Figure 5c** with the connectivity of the pore space in a 2.5x2.5x2x5$\mu m^3$ cube taken from the middle of the packing. **Figure 6** compares the frequency distributions from Eksi's and our works. The average pore sizes (Eksi: 0.133μm, this work: 0.138μm) compare well. However, the distributions have different forms, having tails extending to opposing directions. The difference is probably a result of the tetrahedral pore definition in [15]. The definition imposes a connectivity of 4 to all the pores, which tends to divide large pores into smaller ones. This is well illustrated by the fact that a single pore in cubic packing (Figure 2c) is represented by 6 tetrahedral pores if the pore definition of [15] is used. It seems clear that a pore definition that is based on identifying the minimum in hydraulic radius when moving from one pore to adjacent one, has fewer limitations than previous approaches.

The characterization technique described in present work readily provides the same statistics as earlier techniques with the exception of surface roughness data that is related to particle positions and orientations in the coating top layer rather than the pore space itself. The current analysis technique improves earlier techniques by providing a number of additional statistics, examples of which are shown in Figure 7. **Figure 7a** presents the pore size distribution by volume. This distribution might be more important than the frequency distribution when transport processes in a pore space are to be understood. Pores having radius 0.175μm occupy most volume in the packing. The distribution is wide with a cutoff at pore radius ca. 0.07μm. The surface area distribution in **Figure 7b** is similarly broad centering at 0.5$\mu m^2$. There are some pores with very large surface areas, which indicates the presence of non-isometric pores, since the equivalent spherical pore radii calculated for the largest surface areas are larger than largest pores in the pore size distribution (e.g. Area=1.6$\mu m^2$ $\rightarrow$ $r_{eq}$ $\approx$0.36μm > 0.32μm).

The distribution of connectivity (coordination number) is shown in **Figure 7c**. There is a clear maximum at coordination number 4 with a long tail extending up to 16. **Figure 8** shows example pores having coordination numbers 4 and 9. The pore with the coordination number 4 resembles a tetrahedral pore in hexagonal packing where as coordination number 9 leads to a more complex structure of the pore. **Figure 7d** shows the distribution of coordination number by pore volume. It is evident that most of the pore volume is occupied by pores having coordination numbers in range 4-8, which should be taken into account when modeling transport processes in packed structures such as coating layers. Additional note can be made that there seems to be neither isolated nor dead-end pores in the structure, i.e. pores with coordination numbers less than 2. **Figure 7e** shows the distribution of the connected surface area to the total internal surface area.

The distribution is symmetric and centered around 0.35. No pores seem to have throat areas that are less than 15% or more 60% of the internal pore surface area. The large number of pores in the packing with high connectivities and large throat areas suggest that partial wetting of the pore surfaces prior to pore filling might be important when predicting the flow into the pore space. This is further commented in the companion paper [16].

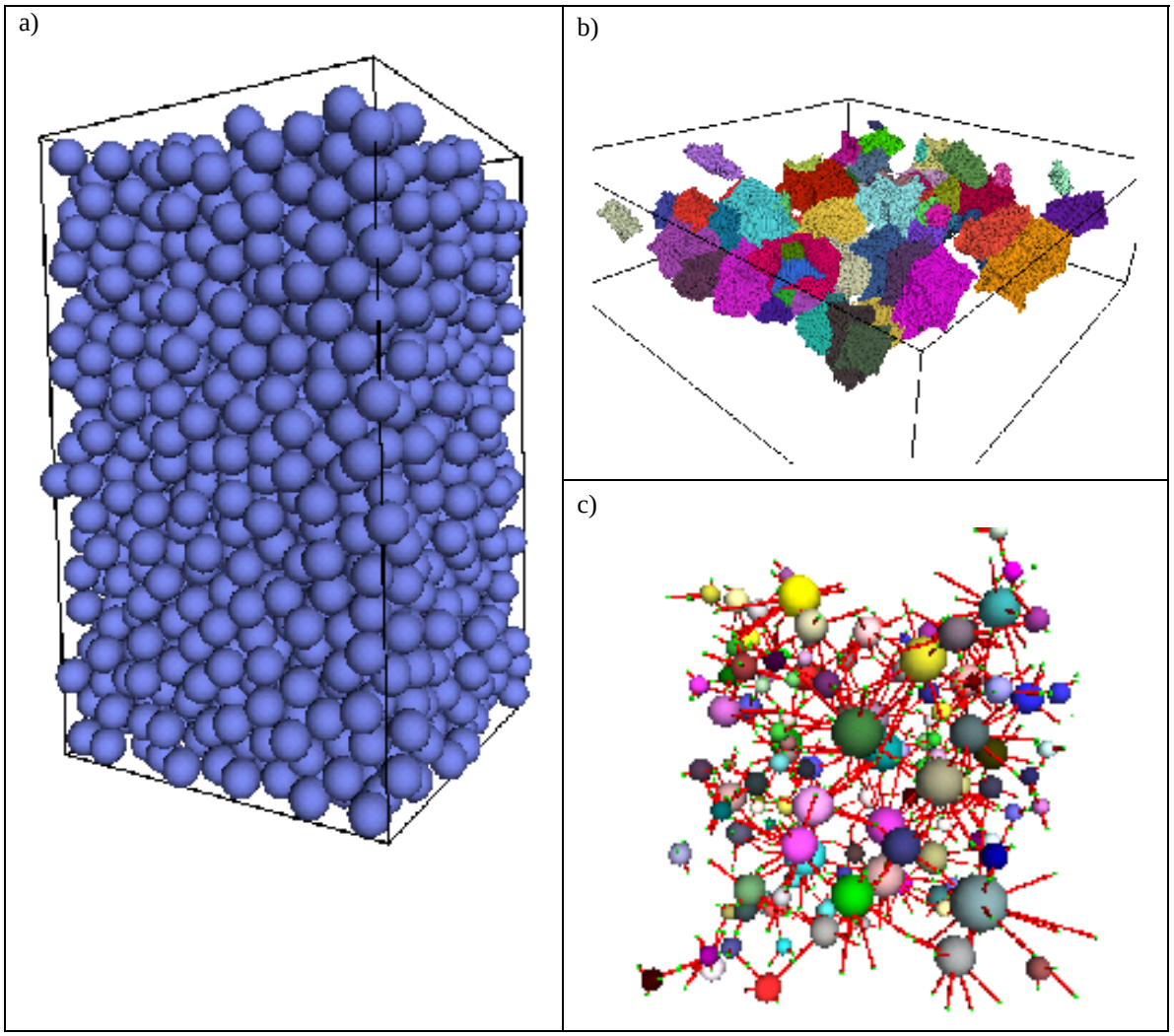


***Figure 5. Monodisperse random packing of 0.5µm diameter spheres. The dimensions of the packing are 5x8.5x5µm$^3$ and porosity is 0.40. A slice through the center of the corresponding pore space (b) and inter-void connections in a 2.5x2.5x2x5µm$^3$ cube (c) taken from the middle are shown to the right.***

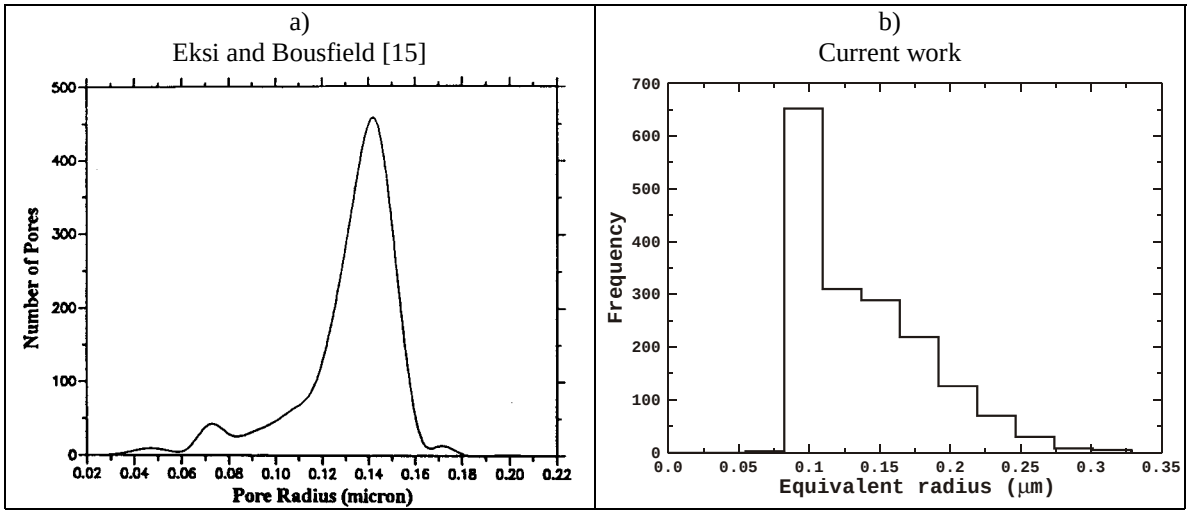


***Figure 6. Comparison of the pore size distributions in [15] and current work. The data is for the packing in Figure 5a.***

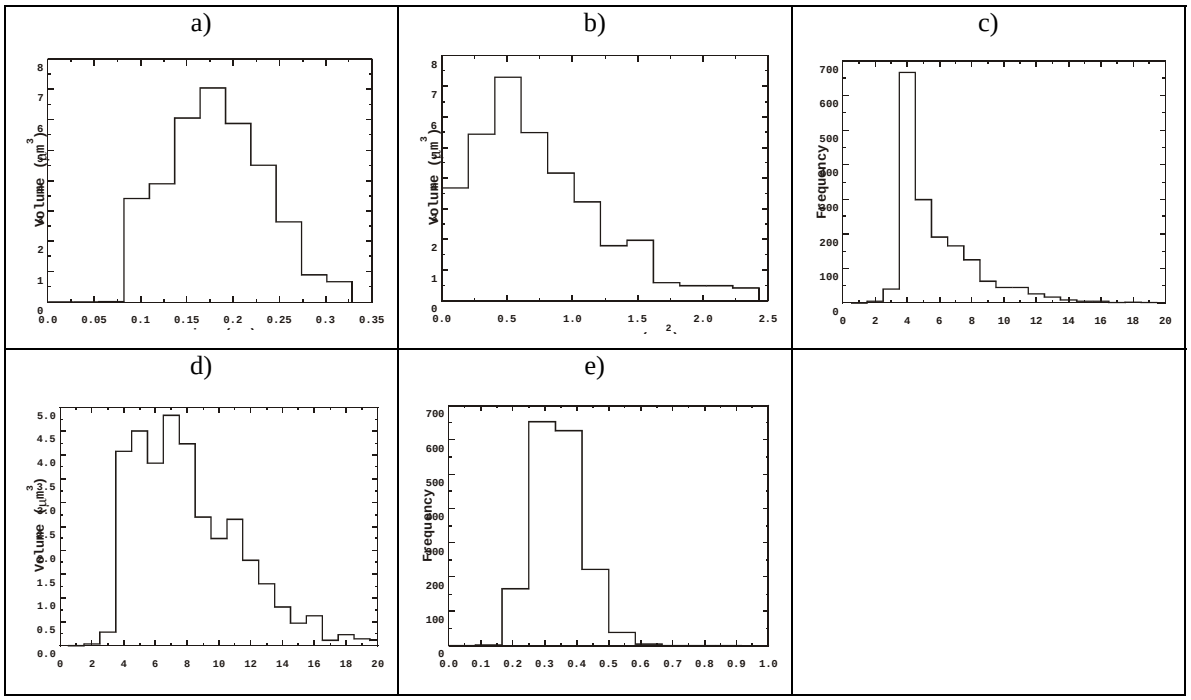


***Figure 7. Pore statistics for the packing in Figure 5a. (a) Pore size distribution. (b) Pore surface area distribution. (c) Coordination number distribution. (d) Pore volume associated with each coordination number. (e) Distribution of the ratio [connected pore surface area]/[internal pore surface area].***

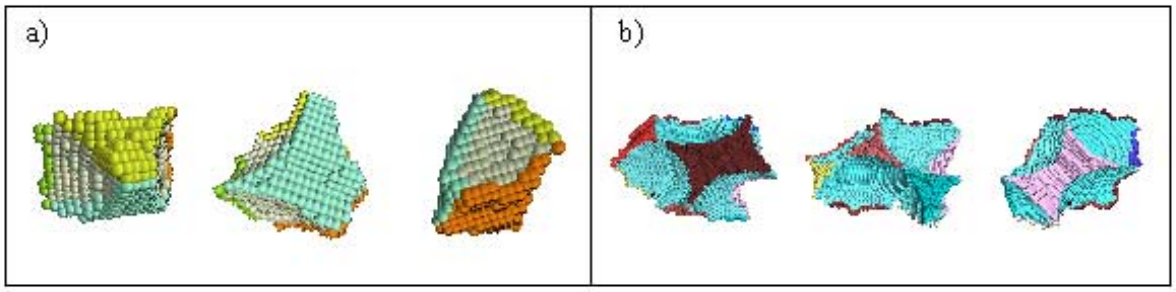


***Figure 8. Example pores from monodisperse random packing. Coordination number is 4 in (a) and 9 in (b). Different shades of gray illustrate surfaces in contact with neighboring pores. Three views from each pore are shown.***

*Pore space in polydisperse model packing*

In order to investigate how a pore space in a packing of polydisperse particles differs from that of a monodisperse one, a model packing using a particle size distribution based on a commercial coating pigment (GCC: 90% < 2μm, **Figure 9a**) was generated and analyzed. The packing structure shown in **Figure 9b** was generated with the same model of Eksi and Bousfield [15] as the monodisperse packing. The porosity of the packing was found to be 0.30, which is in excellent agreement with the experimental value of 0.287 that was reported for the commercial pigment of the same particle size distribution as the model [17]. Experimental porosity was measured for tablets that were compressed with low pressure in dry state. The pore structure of the model packing was analyzed with resolution of 100 voxels per unit length. The results are presented in **Figure 10**.

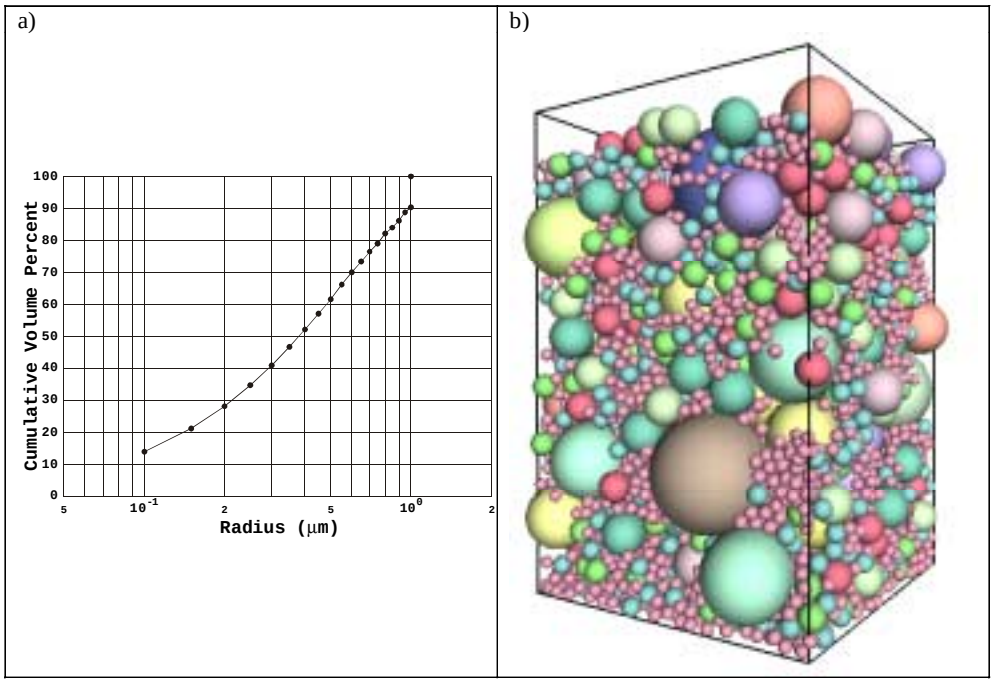


***Figure 9. (a) Particle size distribution for model packing based on a commercial coating pigment. (b) The packed structure corresponding to (a). The dimensions of the packing are 5x8x5μM$^3$ and porosity is 0.30.***

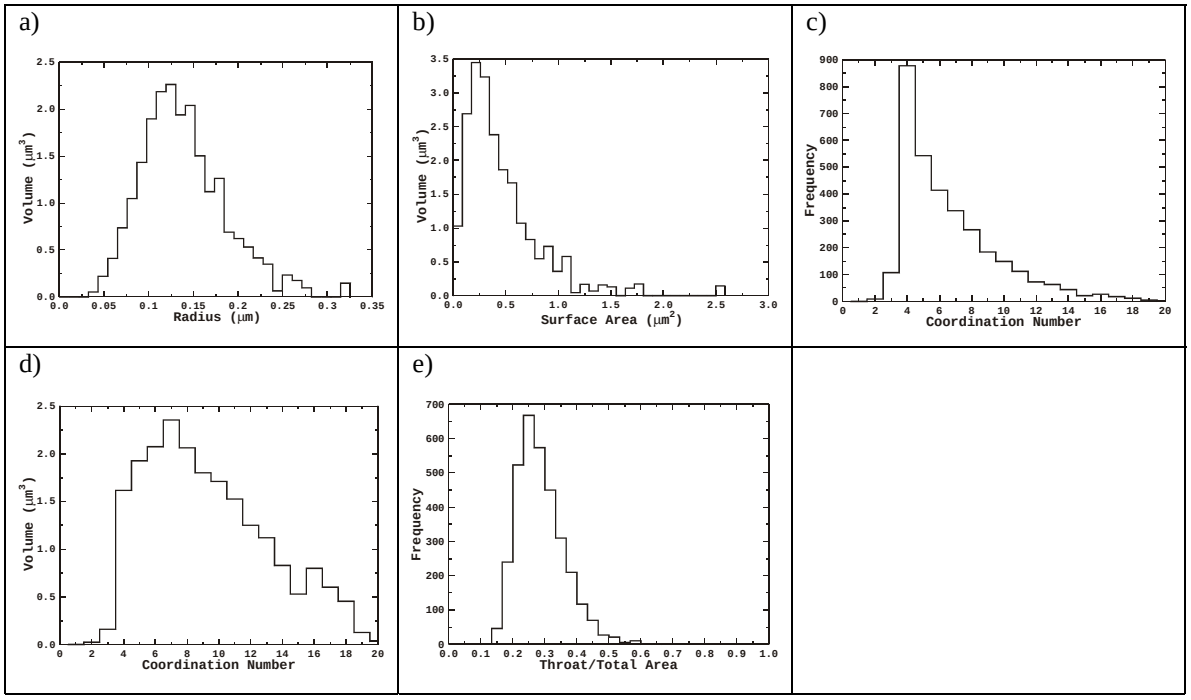


***Figure 10. Pore statistics for the polydisperse packing in Figure 9b. (a) Pore size distribution. (b) Pore surface area distribution. (c) Coordination number distribution. (d) Pore volume associated with each coordination number. (e) Distribution of the ratio [connected pore surface area]/[internal pore surface area].***

The average pore radius is 0.13μm, which can be contrasted to the smallest particle size in the distribution, 0.2μm diameter. For the monodisperse packing of 0.5μm particles the average pore radius was 0.175μm (35% of the diameter). For particles of diameter 0.2μm one expects average poresize to be ca. 0.07μm. Therefore, the average poresize in the polydisperse model packing is larger than expected. The large value is probably caused by the fact that small particles cannot effectively fill all the pore space between the larger particles.

The average pore surface area (Figure 10b) is 0.33$\mu m^2$ and average throat to total surface area (Figure 10e) is 0.27. Both distributions are similar to those of the monodisperse packing. The coordination number distribution (Figure 10c) is also similar to that of the monodisperse case, most common coordination number being 4 with a long tail extending to higher values. Volume distribution of coordination number is slightly broader for the polydisperse case. Pores that have coordination numbers up to 10 and larger occupy a considerable volume of the pore space.

## Fractal analysis

The data obtained with the analysis technique presented in this paper allows one to study fractal characteristics of a pore space. Current work only touches upon this topic to illustrate the possibilities for future research. For previous work and definitions of fractal analysis related to paper and paper coatings see e.g. [18–20].

Fractal dimensions calculated for a pore space can be used to investigate e.g. whether a scaling relationship to the pore size distribution exists. The relationship exists if surface areas of pores $A_i$ and corresponding volumes $V_i$ scale as to some characteristic length $l_i$:

$$A_i \propto l_i^D \propto V_i^{D/3},$$

where $D$ is the fractal dimension. For an Euclidean space $D$=2, and for fractal structures $2 < D <= 3$. If surface area of pores is plotted against cube root of corresponding pore volumes on a log-log scale, the possible fractal nature of a structure can be assessed. **Figure 11a** shows the fractal analysis data for the monodisperse packing in Figure 5a. The data shows a linear relationship with a slope of 2.49. Therefore, we can conclude that the pore structure of monodisperse randomly packed particles does indeed show fractal characteristics. The intrepretation of the fractal dimension in present content is that the small and large pores have different form, i.e. the surface area of the pores increases faster as a function of pore volume than would be expected for an Euclidean object. The large pores have a more complex surface structure when compared to the small pores.

The corresponding log-log plot for the polydisperse packing (Figure 9b) is shown in **Figure 11b**. Also in this case the pore structure shows fractal characteristics with $D$=2.19. The smaller fractal dimension indicates that the small and large pores are more similar in structure in the case of a polydisperse particle size distribution.

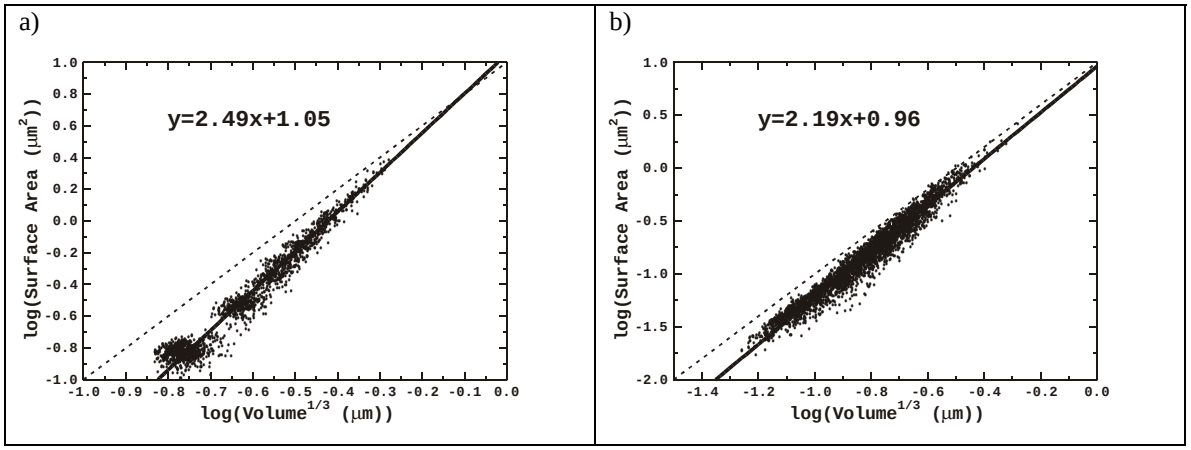


***Figure 11. Fractal analysis of the pore space. (a) Pore surface areas vs. cube root of pore volumes for the monodisperse packing in Figure 5a. (b) same as (a) for the polydisperse packing in Figure 9b. The dotted line corresponds the Euclidean behavior. The equations are linear fits to the data points.***

## CONCLUDING REMARKS

The characterization technique presented in this paper partitions a pore space in a meaningful and useful way and is an improvement over earlier methods. The results provide insight into the microscopic pore structure of paper coatings and help understanding and interpreting properties and end use performance of coated paper.

The accuracy of the method was verified by comparing the results with known properties of ordered mono-sized sphere packings. Computer generated random sphere packings were also analyzed. Results of monodisperse packings agreed with earlier published results and additional information of the pore structure was obtained. In polydisperse model packing that was based on commercial coating pigment the small particles were not able to fill efficiently the pore space formed by the larger particles. For all the random packings the most common coordination number was found to be 4, but a long tail extending to higher coordination numbers was also observed. Pores with coordination numbers in range 4 to 10 occupied most of the volume in the packings. Fractal dimension was found to be larger for the monodisperse packing than the polydisperse one indicating that in former the small and large pores are more dissimilar in form than in latter. Fractal dimensions obtained from the model can be used to identify scaling factors for pore size distributions, which could provide a way to differentiate particle size distributions in a useful way in future.

Present work analyzed void spaces in computer generated model packings. Characterization of real pigment coatings could be possible in future as experimental techniques in computer imaging keep improving. Application to void spaces in base sheets should already be possible with existing techniques. Future work will attempt to propose optimal coating structures consisting of various pigments of varying sizes and forms. Additionally, the topographical model generated by the technique will be used as a starting point for modeling transport processes in porous structures.

## ACKNOWLEDGMENTS

Authors thank Professor D. W. Bousfield for helpful discussions and giving access to the particle packing software of University of Maine. The valuable advice of Dr. P. A. C. Gane of Omya, Plüss-Staufer is greatly appreciated.

## REFERENCES

1. Lepoutre, P., Structure and performance of pigmented coatings: what do we know?, In *Proceedings of 1996 International Paper and Coating Chemistry Symposium*, Ottawa, Canada, p.205.
2. Dullien, F. A. L., *Porous Media - Fluid Transport and Pore Structure*, Academic Press, San Diego, 1992.
3. Kettle, J. P. and Matthews, G. P., Computer Modelling of the Pore Structure and Permeability of Pigmented Coatings, in *Proceedings of TAPPI 1993 Advanced Coating Fundamentals*, TAPPI Press, Atlanta, p.121.
4. Matthews, G. P., Ridgway, C. J. and Spearing, M. C., Void Space Modeling of Mercury Intrusion Hysteresis in Sandstone, Paper Coating, and Other Porous Media, *Journal of Colloid and Interface Science*, 171: 8(1995).
5. Kwiecien, M. J., Macdonald, I. F. and Dullien, F. A. L., Three-dimensional reconstruction of porous media from serial section data, *Journal of Microscopy*, 159(3): 343(1990).
6. Zhao, H. Q., Macdonald, I. F. and Kwiecien, M. J., Multi-Orientation Scanning: A Necessity in the Identification of Pore Necks in Porous Media by 3-D Computer Reconstruction from Serial Section Data, *Journal of Colloid and Interface Science*, 162: 390(1994).

7. Baldwin, C. A., Sederman, A. J., Mantle, M. D., et al., Determination and Characterization of the Structure of a Pore Space from 3D Volume Images, *Journal of Colloid and Interface Science*, 181: 79(1996).
8. Lin, C. and Cohen M. H., Quantitative methods for microgeometric modeling, *Journal of Applied Physics*, 53(6): 4152(1982).
9. Thovert, J. F., Salles, J. and Adler, P. M., Computerized characterization of the geometry of real porous media: their discretization, analysis and interpretation, *Journal of Microscopy*, 170(1): 65(1993).
10. Dullien, F. A. L., Characterization of Porous Media – Pore Level, *Transport in Porous Media*, 6, 581(1991).
11. Graton, L. C., Fraser, H. J., Systematic Packing of Spheres - With Particular Relation to Porosity and Permeability, *The Journal of Geology*, XLIII(8): 785(1935).
12. Cumberland, D. J. and Crawford, R. J., *The Packing of Particles*, Handbook of Powder Technology Vol. 6, Elsevier, Amsterdam, 1987.
13. Coelho, D., Thovert, J.-F. and Adler, P. M., Geometrical and transport properties of random packings of spheres and aspherical particles, *Physical Review E*, 55(2): 1959(1997).
14. Sastry, S., Corti, D. S., Debenedetti, P. G., et. al., Statistical geometry of particle packings. I. Algorithm for exact determination of connectivity, volume, and surface areas of void space in monodisperse and polydisperse sphere packings, *Physical Review E*, 56(5): 5524(1997).
15. Eksi, G., Bousfield, D. W., Modeling of Coating Structure Development, in *Proceedings of TAPPI 1996 Coating Conference*, p.283.
16. Bousfield, D. W., Pellerin, P. and Toivakka, M., Modeling of short time penetration into complex porous structures, in *Proceedings of this conference*, 2000.
17. Gane, P. A. C., Matthews, G. P., Schoelkopf, J., et al., Observing Fluid Transport Into Porous Coating Structures: Some Novel Findings, in *Proceedings of TAPPI 1999 Advanced Coating Fundamentals Symposium*, p.213
18. Kent, H. J., The fractal dimension of paper surface topography, *Nordic Pulp and Paper Research Journal*, 6(4): 191(1991).
19. Ellis, K. and Fripiat, J., Void volume characterization of coated paper, in *Proceedings of TAPPI International Printing and Graphic Arts Conference1996*, p.149.
20. Kaye, B. H., *A random walk through fractal dimensions*, VCH Publishers, New York, NY, 1989, pp. 261.

Received: May 1, 2000
Accepted: October 10, 2000

This paper was accepted for abstracting and publication in the March 2001 issue of *TAPPI JOURNAL*.

*TAPPI Website: www.tappi.org*